VOL. 24, NO. 3, 2025, 270-275
elektrika.utm.my
ISSN 0128-4428

ELEKTRIKA
Journal of Electrical Engineering

Hierarchical Rutile TiO_2 Nanoflowers vs. Anatase TiO_2 Nanoparticles for Enhanced Efficiency in Dye-Sensitized Solar Cell

Nurul Najihah Ishak[1], **Yusri Md Yunos**[1*] and **Mohamed Sultan Mohamed Ali**[2]

[1]Faculty of Electrical Engineering, Universiti Teknologi Malaysia, 81310 UTM Skudai, Johor, Malaysia.
[2] Department of Electrical Engineering, College of Engineering, Qatar University, Doha, Qatar.

[*]Corresponding author: yusri@utm.my

Abstract: Titanium dioxide (TiO_2) nanostructures are critical components in photoanode layer of dye-sensitized solar cell (DSSC), yet the relationship between their morphology and photovoltaic performance remains an area of significant research interest. This study investigates and compares the morphological, structural and photovoltaic properties of anatase TiO_2 nanoparticles (NPs), deposited via screen-printing and rutile TiO_2 nanoflowers (NFs), synthesized through a hydrothermal method for DSSC applications. The results demonstrate that the hierarchical nanoflower architecture of rutile TiO_2 significantly enhances the effective surface area, leading to a power conversion efficiency (PCE) of 4.11%, which substantially outperforms the PCE of 1.19% achieved by anatase TiO_2 NPs. These findings highlight the critical role of morphology in DSSC performance and establish hierarchical rutile TiO_2 nanostructures as promising photoanode materials for high-efficiency DSSC.

Keywords: DSSC, TiO_2, Nanoparticles, Nanoflower, Efficiency

Article History: received 25 March 2025; accepted 10 September; published 22 December 2025
Digital Object Identifier 10.11113/elektrika.v24n3.709

1. INTRODUCTION

Photovoltaic (PV) technologies have progressively advanced into various emerging solar cell technologies since the discovery of the photovoltaic effect by French physicist Edmond Becquerel in 1839, when he observed a voltage generated between the electrodes of an electrochemical cell upon illumination [1]. Emerging solar cells can be broadly classified into four primary types based on their development timeline: organic solar cells (1950s) [2], quantum dot solar cells (QD) (1970s) [3], dye-sensitized solar cell, (DSSC) (1991s) [4], and perovskite solar cells (2012s) [5]. Among these technologies, DSSC have attracted significant attention due to their advantages over other emerging solar cells. Unlike organic and QD solar cells, which suffer from low stability and limited efficiency due to charge recombination and material degradation, DSSC exhibit relatively higher stability and efficiency attributed to their unique photoelectrochemical mechanism [6]. The utilization of a sensitizing dye and semiconductor oxide framework allows for efficient light absorption and charge transfer, enhancing overall performance [7]. Furthermore, DSSC demonstrate more durability compared to perovskite solar cells, which face stability issues arising from moisture sensitivity, thermal instability, and material degradation [8], [9].

DSSC architecture consist of (1) two conductive transparent substrates, (2) a working semiconductor electrode (photoanode) doped with a dye (sensitizer), (3) a redox electrolyte, and (4) a counter electrode (cathode) [10]. Notably, the photoanode layer plays a critical role in determining the overall efficiency of DSSC, as it provides the primary surface area for dye adsorption. The photoanode, typically composed of a semiconductor oxide layer such as titanium dioxide (TiO_2), serves as the substrate for dye molecules to anchor through chemical bonding. A high surface area is crucial as it allows for a greater amount of dye loading, thereby enhancing light absorption efficiency and promoting higher photon-to-current conversion efficiency [11]. TiO_2 exists in three primary polymorphs: anatase, rutile, and brookite [12]. Among these, anatase and rutile are utilized in DSSC applications due to their favorable electronic properties and stability. Anatase TiO_2 nanoparticles (NPs) are widely employed in DSSC owing to their high photocatalytic properties compared to other polymorphs like rutile. This enhanced activity is attributed to its indirect band gap, which leads to longer electron-hole pair lifetimes, thereby increasing the charge carriers participating in photoanode surface reactions. For instance, studies have reported efficiencies of 7.06% using anatase TiO_2 nanoparticles with exposed {001} facets is good potency for dye adsorption and charge transfer [13]. Conversely, rutile TiO_2 nanoflowers (NFs) present several advantages over anatase NPs, particularly in terms of their structural morphology. The hierarchical architecture of rutile TiO_2 NFs provides a larger surface area compared to TiO_2 NPs,

thereby enhancing ultraviolet (UV) light absorption and light-scattering capabilities [14]. Furthermore, the unique NFs can facilitate efficient light trapping and provide direct pathways for electron transport, potentially improving the photovoltaic performance of DSSC. Concurrently, the highest rutile TiO_2 NFs exhibit efficiency of 14.21% using organic betanin dye, demonstrating that the aggregated bunches of NFs offer a large active surface area and greater absorption of incident photons [15].

Therefore, engineering the photoanode layer to maximize surface area is crucial for enhancing the overall photovoltaic performance of DSSC. This can be achieved through various techniques, including physical methods, chemical synthesis, biological approaches, or hybrid strategies that integrate multiple methodologies [16]. Therefore, this study aims to conduct a preliminary comparative analysis of anatase TiO_2 NPs using screen-printing method and rutile TiO_2 NFs using hydrothermal method as photoanode materials in DSSC, focusing on their morphological, elemental, structural and electrical properties.

2. EXPERIMENTAL METHOD

2.1 Preparation of titania morphology

The anatase TiO_2 NPs were obtained from commercial titania of Ti-Nanoxide T/SP on the fluorine-doped tin oxide (FTO) glass substrates with dimensions of 2.5 cm × 1.5 cm and a resistivity of 8 Ω/cm^2 (Solaronix, Switzerland) using screen-printing method. During the screen-printing process, the Ti-Nanoxide T/SP paste was uniformly applied onto the FTO glass substrate by smoothly moving a squeegee across the area framed by Scotch tape to ensure consistent thickness and coverage. After the deposition, the TiO_2-coated FTO glass substrates were annealed at 475°C for 30 minutes to enhance the adhesion of the TiO_2 film.

In contrast, the rutile TiO_2 NFs were synthesized via a hydrothermal method, as described in a previous study [17]. In this process, titanium (IV) butoxide (TBOT, 97% purity, Sigma Aldrich, China) was added dropwise to a solution of hydrochloric acid (HCl, 36%–38% purity, J.T. Baker, Thailand) and deionized (DI) water (18.2 MΩ, Milli-Q Ultrapure) under vigorous stirring to ensure homogeneity. The resulting mixture was transferred to a Teflon-lined stainless-steel autoclave and heated at 150°C for 10 hours to facilitate the growth of rutile TiO_2 NFs. After the hydrothermal reaction, the synthesized samples were collected, washed repeatedly with DI water to remove residual impurities, and dried at room temperature.

For the fabrication of DSSC, both the anatase TiO_2 NPs and rutile TiO_2 NFs were employed as photoanodes layer. The prepared photoanode layers were immersed in an N719 dye solution for 24 hours to allow dye adsorption. After immersion, the samples were rinsed with ethanol to remove any unbound dye molecules from the surface. Subsequently, the dye-sensitized photoanode and a platinum (Pt) counter electrode were assembled in a sandwich configuration using binder clips. Finally, the redox electrolyte (iodide/triiodide) was injected into the inter-electrode space to complete the DSSC assembly. A schematic representation of the DSSC fabrication process is illustrated in Figure 1.

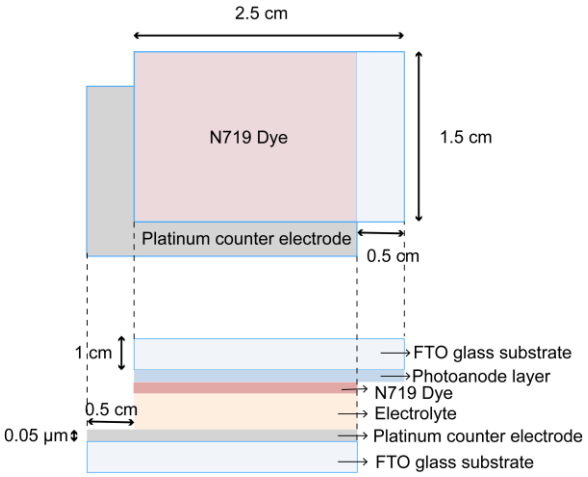

Figure 1. DSSC sandwich configuration

2.2 Characterization Method

The morphology of the anatase TiO_2 NPs and rutile TiO_2 NFs samples was characterized using a JSM-7600F field-emission scanning electron microscope (FESEM) (JEOL, Tokyo, Japan) equipped with energy-dispersive X-ray spectroscopy (EDS) to analyze the elemental composition of the samples. The structural properties and crystalline phases of the prepared samples were examined through X-ray diffraction (XRD) analysis using a Rigaku SmartLab Advance X-ray diffractometer (Rigaku, Japan) with Cu Kα radiation (λ = 1.5408 Å). The XRD patterns were recorded over a scanning range of 25° to 80° to identify and confirm the polymorphic phases of TiO_2 present in the samples. The efficiency of DSSC device is measured using a solar simulator (AM-1.5 G, Newport Oriel, Newport Stratford Inc. USA) connected with a Keithley model 2400 source meters.

3. RESULT AND DISCUSSIONS

This section describes the morphology, elemental, structural and electrical properties of prepared samples.

3.1 Morphology and Elemental Properties

The morphological and elemental characteristics of bulk anatase TiO_2 NPs and rutile TiO_2 NFs are shown in Figure 2 (a) and (b), respectively. In Figure 2 (a), the anatase TiO_2 NPs sample demonstrates a granular, quasi-spherical morphology, with approximately particles averaging ~10 nm in diameter that aggregate into larger clusters due to interparticle van der Waals interactions [18]. In contrast, Figure 2(b) demonstrates the hierarchical nanoflower architecture of rutile TiO_2 NFs, composed of radially aligned, petal-like nanosheets. This three-dimensional structure can increase the effective surface area for dye adsorption and enhance light-scattering capabilities within the cell, thereby promoting more efficient light absorption.

Elemental composition analysis via EDS revealed deviations from the ideal TiO_2 stoichiometry (Ti:O = 1:2). For anatase TiO_2 NPs (Figure 2a), the Ti and O contents

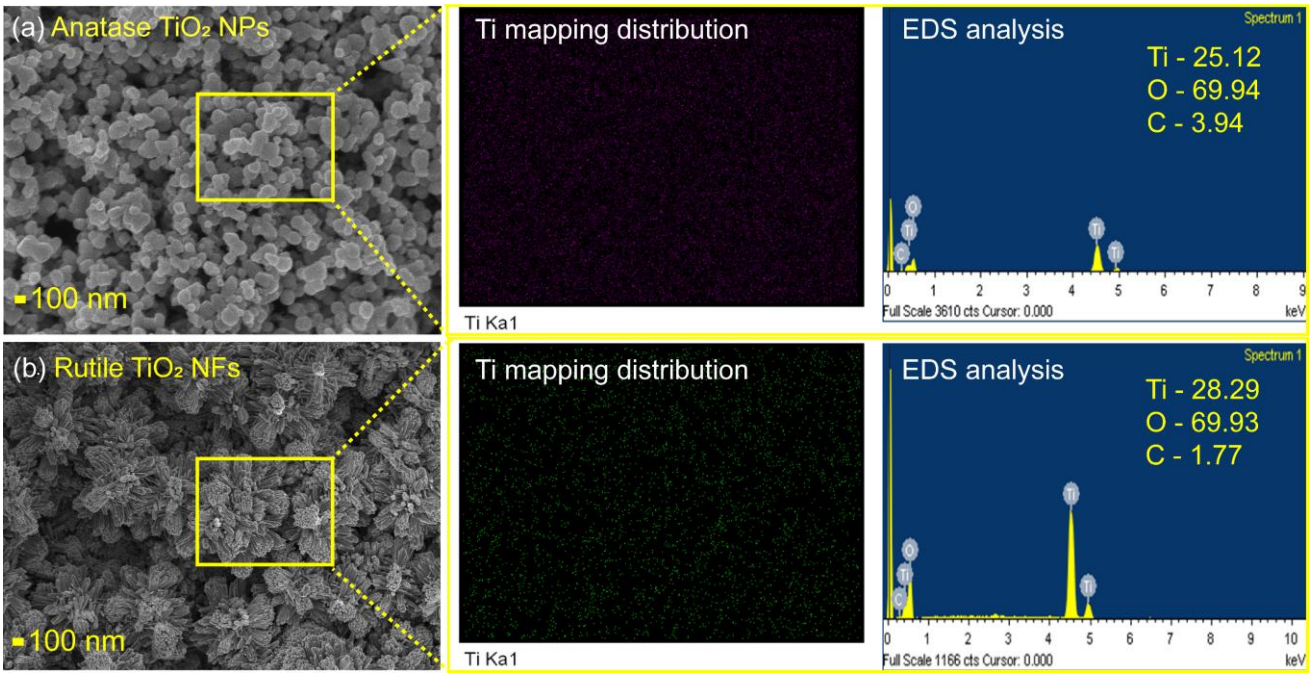

Figure 2. (a) FESEM image of anatase TiO_2 NPs, Ti mapping distributions of anatase TiO_2 NPs, EDS analysis of anatase TiO_2 NPs and (b) FESEM image of rutile TiO_2 NFs, Ti mapping distributions of rutile TiO_2 NFs, EDS analysis of rutile TiO_2 NFs.

were quantified as 25.12 wt% and 69.94 wt%, respectively, yielding an atomic ratio of Ti:O ≈ 1:8.3. The rutile TiO_2 NFs (Figure 2e–f) exhibited a higher Ti content (28.29 wt%) and comparable O content (69.93 wt%), resulting in a Ti:O atomic ratio of ≈1:7.3. The excess oxygen content in both samples may arise from adsorbed surface species (e.g., hydroxyl groups or moisture) or measurement artifacts due to carbon tape interference (evidenced by residual carbon signals: 3.94 wt% for anatase, 1.77 wt% for rutile). Notably, the rutile phase's elevated Ti content and uniform Ti distribution (Figure 2b) align with its denser crystalline framework and reduced oxygen vacancy concentration compared to anatase.

Based on these morphological and elemental analyses, rutile TiO_2 NFs appear to offer distinct advantages over anatase TiO_2 NPs for DSSC applications. The hierarchical, petal-like architecture of the nanoflowers provides a larger surface area for dye adsorption and enhances light scattering, which are efficient for photon capture. Additionally, the denser crystalline framework suggested by the higher Ti content in rutile may contribute to robust structural integrity and improved device performance. Although anatase TiO_2 NPs are well-established and exhibit favorable electron transport properties, the three-dimensional arrangement of rutile TiO_2 NFs can enhance light-absorption capabilities, potentially leading to higher efficiencies of DSSC.

3.2 Structural Analysis

Figure 3(a) presents the XRD pattern of anatase TiO_2 NPs, with peaks corresponding to the (101), (103), (004), (200), (202), (105), (213), and (203) crystallographic planes. The prominent peaks observed at 25.37° and 37.87° confirm the formation of a pure anatase phase, with no detectable impurity phases. These diffraction peaks are consistent with the reference pattern (ICDD No. 98-008-2082), as verified using HighScore software, and supported by previous studies [19], [20]. The indexed planes confirm the pure tetragonal anatase phase of TiO_2 NPs with the octahedral and trigonal planar coordination geometry.

In Figure 3(b) depicts the XRD pattern of rutile TiO_2 NFs, revealing strong diffraction peaks at 27.41°, 35.97°, 41.12°, and 54.06°, which correspond to the (110), (101), (111), and (211) crystallographic planes, respectively. Additional lower-intensity peaks at (210), (002), (301), and (112) further confirm the rutile phase. This result aligns well with ICDD No. 98-003-9167 and previous research, indicating that the sample predominantly consists of the rutile phase of TiO_2. In the context of DSSC applications, anatase TiO_2 NPs are typically preferred due to its higher conduction band edge and efficient electron transport properties, which collectively minimize recombination losses. However, rutile TiO_2, particularly in its hierarchical nanoflower morphology, can exhibit enhanced performance under specific conditions. This is attributed to its superior light-scattering capabilities and larger effective surface area, both of which are critical for optimizing photon absorption and overall device efficiency [21].

3.3 Electrical Properties and Thickness

Figure 4 shows the photocurrent density–voltage (*J–V*) curves for DSSC fabricated with anatase TiO_2 NPs and rutile TiO_2 NFs under simulated solar illumination (AM 1.5, 100 mW cm^{-2}). The power conversion efficiency

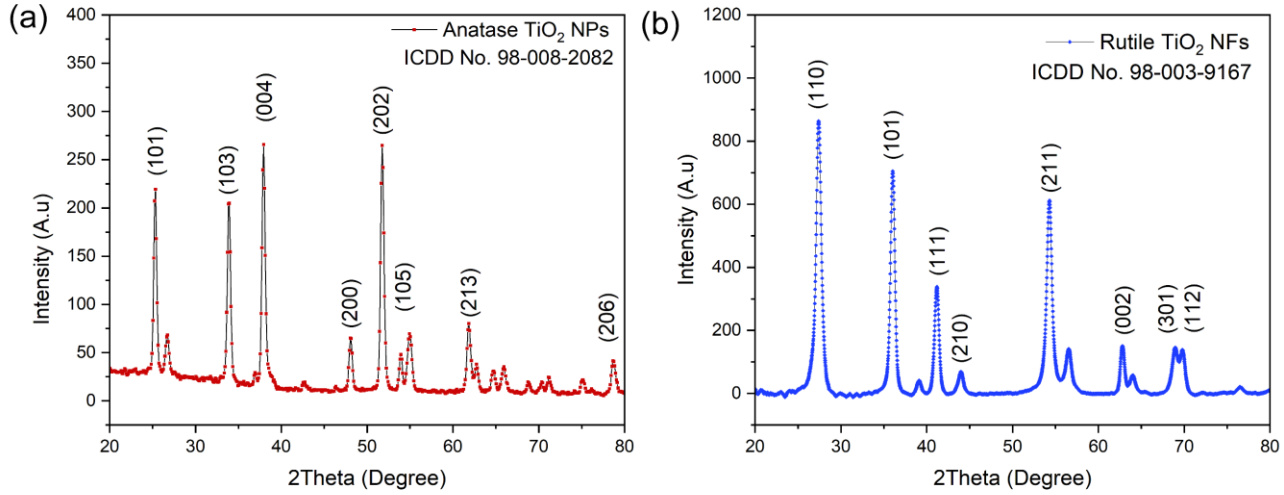

Figure 3. X-ray diffraction analysis. (a) anatase TiO_2 NPs, (b) rutile TiO_2 NFs

(PCE, η) of the devices was calculated using Equation (1) [22]:

$$\eta = \frac{V_{OC} \times J_{SC} \times FF}{P_{in}} \quad (1)$$

where η is the power conversion efficiency (PCE), V_{OC} (in volt) is the open-circuit voltage, J_{SC} (mA/cm^2) is the short-circuit photogenerated current density, FF is the fill factor, and Pin is the power of incident light (photon) per unit area.

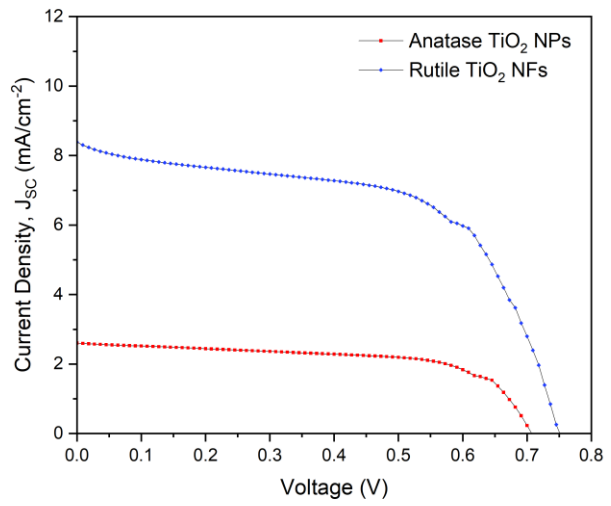

Figure 4. Photovoltaic characteristics of anatase TiO_2 NPs and rutile TiO_2 NFs.

The DSSC fabricated with anatase TiO_2 NPs demonstrated a PCE of 1.19%, with a J_{SC} of 2.61 mA cm^{-2}. In contrast, the DSSC fabricated with rutile TiO_2 NFs achieved a significantly higher PCE of 4.11%, accompanied by a of J_{SC} 8.36 mA cm^{-2}. This notable enhancement in performance can be attributed to the hierarchical nanoflower morphology of rutile TiO_2 NFs, which provides a larger effective surface area compared to the nanoparticle structure. The increased surface area facilitates greater dye adsorption, enhancing light absorption and improving charge carrier generation [15]. Additionally, the unique morphology of rutile TiO_2 NFs with interconnected network of petal-like nanosheets has promoted efficient electron transport and reduces recombination losses, further contributing to enhance photovoltaic performance. The resulting photovoltaic parameters are summarized in Table 1.

Table 1. Comparison of photovoltaic parameters between anatase TiO_2 NPs and rutile TiO_2 NFs.

Sample	Anatase TiO_2 NPs	Rutile TiO_2 NFs
Physical Properties	Spherical nanoparticles	Hierarchical nanoflowers
EDS Composition	Ti: 25.12% O: 69.94% C: 3.94% (contamination)	Ti: 28.29% O: 69.93% C: 1.77% (contamination)
V_{OC} (V)	0.71	0.74
J_{SC} (mA/cm^{-2})	2.61	8.36
FF	63.51	65.91
PCE (%)	1.19	4.11

4. CONCLUSION

This study investigated the morphological and structural properties of anatase TiO_2 NPs and rutile TiO_2 NFs were investigated to evaluate their impact on photovoltaic performance in DSSC. Anatase TiO_2 NPs fabricated via a screen-printing method, exhibited nanoparticle morphology, while rutile TiO_2 NFs synthesized through a hydrothermal approach shows hierarchical nanoflower architecture. The nanoflower morphology significantly enhanced the effective surface area of rutile TiO_2 NFs, enabling greater dye adsorption and light absorption

capabilities. The DSSC fabricated with rutile TiO_2 NFs achieved PCE of 4.11%, significantly outperforming the anatase TiO_2 NPs-based device (PCE = 1.19%). The rutile TiO_2 NFs highlights the importance of morphology in influencing charge transport and recombination dynamics. The interconnected network of rutile NFs facilitated efficient electron transport and reduced recombination losses, whereas the dense packing and limited surface area of anatase NPs likely impeded effective charge extraction. These findings underscore the potential of hierarchical rutile TiO_2 NFs as highly promising photoanodes for DSSC. Future research should explore the integration of rutile TiO_2 NFs with conductive interlayers such as MXene to further enhance charge separation and light absorption. Additionally, tailoring surface chemistry and optimizing interface engineering with solid-state or gel electrolytes may help minimize series resistance and improve DSSC stability.

ACKNOWLEDGMENT

This work was supported by Ministry of Higher Education under Fundamental Research Grant Scheme FRGS/1/2022/TK07/UTM/02/42 and Universiti Teknologi Malaysia under UTM Fundamental Research Grant Q.J130000.3823.22H55.

REFERENCES

[1] S. R. Wenham and M. A. Green, "Silicon solar cells," *Prog. Photovoltaics Res. Appl.*, vol. 4, no. 1, pp. 3–33, 1996, doi: 10.1002/(SICI)1099-159X(199601/02)4:1<3::AID-PIP117>3.0.CO;2-S.

[2] G. A. Chamberlain, "Organic solar cells: a review," vol. 8, pp. 47–83, 1983.

[3] M. C. Beard, J. M. Luther, and A. J. Nozik, "Multiple exciton generation in semiconductor quantum dots and electronically coupled quantum dot arrays for application to third- generation photovoltaic solar cells," *Colloid. Quantum Dot Optoelectron. Photovoltaics*, vol. 9780521198, pp. 112–147,2010, doi: 10.1017/CBO9781139022750.006.

[4] B. O'Regan and M. Grätzel, "A Low-Cost, High-efficiency Solar Cell Based on Dye-sensitized Colloidal TiO_2 Films," *Nature*, vol. 353, p. 737, 1991.

[5] J. Y. Kim, J.-W. Lee, H. S. Jung, H. Shin, and N.-G. Park, "High-Efficiency Perovskite Solar Cells," *Chem. Rev.*, vol. 120, no. 15, pp. 7867–7918, 2020, doi: 10.1021/acs.chemrev.0c00107.

[6] A. N. B. Zulkifili, T. Kento, M. Daiki, and A. Fujiki, "The Basic Research on the Dye-Sensitized Solar Cells (DSSC)," *J. Clean Energy Technol.*, vol. 3, no. 5, pp. 382–387, 2015, doi: 10.7763/jocet.2015.v3.228.

[7] W. N. Bahutair, A. Alhajar, A. Al Othman, and M. Tawalbeh, "The role of MXenes and MXene composites in enhancing dye-sensitized solar cells characteristics," *Process Saf. Environ. Prot.*, vol. 191, no. September, pp. 490–504, 2024, doi: 10.1016/j.psep.2024.09.008.

[8] X. Li *et al.*, "Dimensional diversity (0D, 1D, 2D, and 3D) in perovskite solar cells: exploring the potential of mixed-dimensional integrations," *J. Mater. Chem. A*, vol. 12, no. 8, pp. 4421–4440, 2024, doi: 10.1039/d3ta06953b.

[9] J. Prakash *et al.*, "Progress in tailoring perovskite based solar cells through compositional engineering: Materials properties, photovoltaic performance and critical issues," *Mater. Today Energy*, vol. 9, pp. 440–486, 2018, doi: 10.1016/j.mtener.2018.07.003.

[10] C. Lin *et al.*, "Tailoring the Structure–Property Relationships of Innovative Flowerlike TiO_2 Structures in a Fiber-Shaped Dye-Sensitized Solar Cell," *ACS Appl. Energy Mater.*, vol. 7, no. 6, pp. 2329–2337, Mar. 2024, doi: 10.1021/acsaem.3c03091.

[11] S. Bai *et al.*, "Advancements in the development of various types of dye-sensitized solar cells: A comparative review," *Energy Eng. J. Assoc. Energy Eng.*, vol. 118, no. 4, pp. 737–759, 2021, doi: 10.32604/EE.2021.016157.

[12] N. G. Park, J. Van De Lagemaat, and A. J. Frank, "Comparison of dye-sensitized rutile- and anatase-based TiO_2 solar cells," *J. Phys. Chem. B*, vol. 104, no. 38, pp. 8989–8994, 2000, doi: 10.1021/jp9943651.

[13] L. Chu, Z. Qin, J. Yang, and X. Li, "Anatase TiO_2 Nanoparticles with Exposed {001} Facets for Efficient Dye-Sensitized Solar Cells," *Sci. Rep.*, vol. 5, pp. 1–10, 2015, doi: 10.1038/srep12143.

[14] M. Ye, H. Y. Liu, C. Lin, and Z. Lin, "Hierarchical rutile TiO_2 flower cluster-based high efficiency dye-sensitized solar cells via direct hydrothermal growth on conducting substrates," *Small*, vol. 9, no. 2, pp. 312–321, 2013, doi: 10.1002/smll.201201590.

[15] N. D. Desai, K. V. Khot, T. Dongale, K. P. Musselman, and P. N. Bhosale, "Development of dye sensitized TiO_2 thin films for efficient energy harvesting," *J. Alloys Compd.*, vol. 790, pp. 1001–1013, 2019, doi: 10.1016/j.jallcom.2019.03.246.

[16] S. J. Lee, H. Jang, and D. N. Lee, "Recent advances in nanoflowers: compositional and structural diversification for potential applications," *Nanoscale Adv.*, vol. 5, no. 19, pp. 5165–5213, 2023, doi: 10.1039/d3na00163f.

[17] N. N. Ishak, N. Nayan, M. M. Ikhsan Megat Hasnan, M. Nafea, Y. M. Yunos, and M. S. Mohamed Ali, "Nanothorn Photoanodes: A New Approach for Efficiency Enhancement in Dye-Sensitized Solar Cells," *Proc. IEEE Conf. Nanotechnol.*, vol. 2023-July, pp. 893–898, 2023, doi: 10.1109/NANO58406.2023.10231264.

[18] M. Kaliva and M. Vamvakaki, *Nanomaterials characterization*. 2020.

[19] R. S. Dubey, K. V. Krishnamurthy, and S. Singh, "Experimental studies of TiO_2 nanoparticles synthesized by sol-gel and solvothermal routes for DSSCs application," *Results Phys.*, vol. 14, p. 102390, 2019, doi: https://doi.org/10.1016/j.rinp.2019.102390.

[20] M. Ghadiry, M. Gholami, C. K. Lai, H. Ahmad, and W. Y. Chong, "Ultra-sensitive humidity sensor based on optical properties of graphene oxide and nano-anatase TiO_2," *PLoS One*, vol. 11, no. 4, pp. 1–14, 2016, doi: 10.1371/journal.pone.0153949.

[21] N. N. Ishak, N. Nayan, M. M. I. Megat Hasnan, N. K. Abd Hamed, Y. Md Yunos, and M. S. Mohamed Ali,

"$SrSnO_3$ Perovskite post-deposition on Ag-doped TiO_2 rutile nanoflower for optoelectronic application," *Mater. Chem. Phys.*, vol. 301, no. February, 2023, doi: 10.1016/j.matchemphys.2023.127608.

[22] M. Roudgar-Amoli, A. Alizadeh, E. Abedini, and Z. Shariatinia, "Delafossite $CuCoO_2$/ZnO derived from ZIF-8 heterojunctions as efficient photoelectrodes for dye-sensitized solar cells," *RSC Adv.*, vol. 13, no. 22, pp. 14825–14840, 2023, doi: 10.1039/d3ra01595e.